JOURNAL OF AIRCRAFT
Vol. 43, No. 3, May–June 2006

Diagnostics of Tool–Part Interactions During Riveting on an Aluminum Aircraft Fuselage

Timothy J. Johnson,* Raymond Manning,† Douglas E. Adams,‡ and Ronald Sterkenburg§
Purdue University, West Lafayette, Indiana 47907-2031
and
Kumar Jata¶
U.S. Air Force Research Laboratory, Wright–Patterson Air Force Base, Ohio 45433

Manufacturing processes including cutting, grinding, polishing, and riveting in metal structures involve dynamic processing loads, which can seriously affect material quality—for example, short transverse stresses or defect densities surrounding rivet holes. In structural health monitoring, these process loads are often not considered when designing loads and usage monitoring sensing and data interrogation systems. Riveting operations for assembling aerostructures and their effects on local material/part quality in the neighborhood of the holes are examined herein. Physics-based nonlinear dynamic models taking into account complex double riveting impacts at the front and back of a fuselage section and the effects of operator preload are first developed to guide the experimental measurement process. Experimental shock acceleration data on the end of a rivet gun are then utilized to extract features for assessing rivet fitness in situ using vibration signals. A qualitative agreement between the analytical and experimental nonlinear resonance data surrounding 100 Hz is obtained. It is demonstrated using rivet quality assurance indicators based on spectral transmission through the tool–part interface and human operator specifications that such techniques can be utilized to identify riveting processes with skewed delivery (gun or bar), circular indentations, and bucking bar slip to assess susceptibility to future damage in fuselage structures. A simple method for normalizing loads data to take into account changes in rivet gun mass is also proposed.

I. Introduction

STRUCTURAL health monitoring (SHM) is a continuous engineering measurement process by which loads and damage in engineering systems are identified to support timely predictions of structural capability. Diagnostic algorithms are used to identify loads and detect, locate, and quantify degradation; prognostic algorithms are used to make future life predictions in real time. A fundamental difference between SHM and traditional nondestructive evaluation (NDE) techniques is that SHM is implemented globally online in an integrated manner using onboard transducers and data interrogation and modeling and simulation hardware and software, whereas NDE is implemented locally and offline. The advantage of identifying loads and degradation online is that important events, for example, impacts or shearing during processing, over the life of structural materials are not missed between scheduled inspections. If critical static (residual stress) and dynamic (overload) input loads are not observed when they occur, then inverse methods for diagnosing the effects of loading cannot make full use of engineering design and analysis data.

For example, impact tests are routinely used to assess the reliability of composite structural components in aircraft by exerting surface impacts and measuring residual strength in destructive tests subsequent to these impacts. If the location and magnitude of impacts throughout an aircraft's entire life cycle are not identified through SHM, then engineering design impact test data are of little use in assessing impact damage and predicting remaining life. Although many researchers have developed loads and usage SHM technologies for the operational life cycle of structural systems, less research has focused on the loads incurred before deployment during the development life cycle involving manufacturing and assembly processes.

In particular, fastener technologies such as rivets are routinely used in aircraft to assemble fuselage structures from constituent components across joints and interfaces. Although most manufacturers use automated processes to assemble new aircraft, most repair patch work in the field is conducted using manual riveting. Both the rivet gun and bucking bar in manual riveting operations exert dynamic loads on fuselage panels over a broad frequency range around fastener holes, which are areas with high geometric stress concentrations. If these loads could be identified during riveting, then this data could be converted into information regarding good/poor quality riveting and potentially be used to manage the structural life cycle. For example, if a dozen or so unusually harsh riveting loads were identified during assembly, then this information could be used to guide future ground inspections of aircraft, requiring inspectors to focus on those areas most susceptible to future degradation. Exceptionally poor rivets could be replaced immediately, but rivet removal also puts stress on an airframe, and marginal rivets are often better over the long term than adding patches to the fuselage to cover rivet removal holes.

This paper develops an SHM technique for classifying manual rivet operations as acceptable or unacceptable based on gun barrel dynamic acceleration response data acquired during riveting. Background information regarding aircraft riveting technology is provided in Sec. II. The objectives and approach are then given in Sec. III, followed by the experimental procedure in Sec. IV, and results in Sec. V. Conclusions regarding use of the method in practice are provided in Sec. VI.

II. Background

Solid rivets have been used for many years in the aerospace industry, and little has changed in the riveting process since World War II. Rivets are still used because the aluminum skins of modern

Received 16 April 2005; revision received 7 October 2005; accepted for publication 11 October 2005.

*Graduate Student, Department of Mechanical Engineering, Ray W. Herrick Laboratories, 140 South Intramural Drive.
†Undergraduate Student, Department of Mechanical Engineering, Ray W. Herrick Laboratories, 140 South Intramural Drive.
‡Associate Professor, Department of Mechanical Engineering, Ray W. Herrick Laboratories, 140 South Intramural Drive.
§Assistant Professor, Department of Aviation Technology, Terminal 273.
¶Technical Advisor, Materials and Manufacturing Directorate.

aircraft are made of 2000/7000 series aluminum alloys, which are strong due to heat treating and artificial aging processes but susceptible to weakening at welding temperatures above 650°F (340°C). Solid rivets are also relatively easy to inspect compared to a weld or bond, and rivets are also relatively inexpensive to install.

Rivets are typically divided into two types: protruding head and flush head rivets. Protruding head rivets are used in areas that are not aerodynamically critical, and flush head rivets are used if a smooth skin is required to reduce drag. The quality of a riveted joint depends on perfect hole preparation and correct installation of the rivets within approximately 3 s. The shank length of the rivet should be 1.5 times the rivet diameter, and after installation the bucked head should extend through the hole 0.5 times the rivet diameter.

Two disadvantages of manual riveting are that operators may become injured, for example, carpal tunnel and white knuckle, and manual riveting requires great skill. In large aircraft production, the use of automated fastener installation technology is increasing, especially in wing construction. In this process, fastener holes are drilled, reamed, and cold worked, and the rivets are installed. All aircraft repair work, however, still uses manual riveting.

Researchers who study aging aircraft agree that materials used for construction of older aircraft are not optimum with respect to corrosion resistance and fatigue, for example, 7075-T6/7178 alloys have poor corrosion resistance compared to newer alloys such as 7050-T76. It is also true that stress corrosion cracking, exfoliation corrosion, and fatigue cracking almost always initiate at fastener/rivet holes. Although plate/sheet and structure thickness are important, rivet parameters such as choice of rivet material and temper, diameter, and length, as well as the riveting process parameters such as forming/preload, skewness, and hole fill, are extremely critical for durability and damage tolerance.

An optimum riveting process will set up beneficial compressive stresses, which can extend fatigue life and provide resistance to stress corrosion crack initiation. A poor rivet process can set up short-transverse stresses that accelerate stress corrosion cracking and fatigue. A thorough understanding of the riveting process became important during the mid-1970s when a large body of data was gathered for C5 aircraft that encountered fatigue problems. A significant amount of U.S. Air Force funded research in that era led to 1) the understanding of beneficial effects of compressive hoop stresses[1,2] around the bore, 2) the usage of interference fit fasteners, and 3) the development of the split sleeve cold expansion process[3] as a repair process to rework existing fastener holes with fatigue damage.

Recently, there has been a resurgence in fundamental studies of riveting of newer aircraft materials[4] to understand the effect of the rivet process parameters. The new aircraft alloys (Al–Li alloys) and fiberglass laminates, for example, aramid aluminum laminate, are sensitive to material chemical composition and material processing; improper processing can introduce poor short-transverse mechanical properties in spite of the materials' superior fatigue crack growth resistance. In the case of fiber metal laminate materials, an improper choice of rivet process parameters can result in delaminations along the metal–fiber laminates.[4] Thus, a scientific SHM approach as discussed in this paper to assess rivet quality would be timely for metal–metal and metal–composite joints.

III. Objectives and Approach

The objectives of this research are to: 1) develop a simplified, qualitative physics-based model of manual rivet gun operations to examine the nonlinear dynamic interactions between the rivet gun, bucking bar, and rivet and to determine the feasibility of a vibration-based SHM measurement and data interrogation methodology for extracting features that can be used to diagnose rivet process quality relative to rivet processes with known good quality; 2) express the rivet process quality feature set in quantifiable terms using geometric objects in parameter space for distinguishing bad-quality processes from good-quality processes; and 3) accommodate variability in the processing dynamics from riveter to riveter and gun to gun. The physics-based model and simulation results, experimental approach, data interrogation procedure, and rivet process quality characterization results for one rivet gun are reported in this paper.

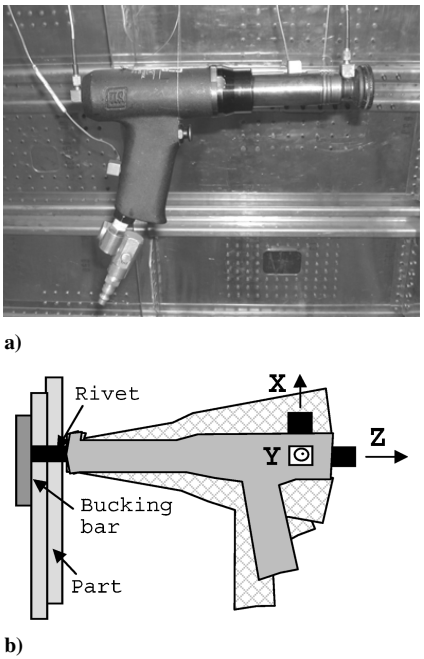

Fig. 1 Photograph of a) pneumatic rivet gun used in experiments and schematic b) of tool–part components at interface with shock accelerometer measurement locations and directions.

A photograph and schematic of the rivet gun studied in this research are shown in Figs. 1a and 1b, respectively. The gun shown in Fig. 1a is suspended with a free–free boundary condition in the barrel direction (Cartesian coordinate Z direction). The X direction is vertical (normal to the barrel), and the Y direction is horizontal (normal to the barrel). The relative positions of the rivet, part, and bucking bar are also shown in Fig. 1b. When the pneumatic trigger on the gun is depressed, an internal, relatively small, free mass, or piston, pulsates against the rivet head at the working end of the gun. These pulsations hammer the rivet into the hole in the overlapped parts to be assembled; a bucking bar that is usually held in place by a second operator on the opposite side of the fuselage acts as an anvil to swage the rivet and create a secure joint. Good riveting operations must avoid the following common errors and last less than 3 s: 1) gun not straight on rivet head resulting in damage to aircraft skin (eyebrows); 2) removal of bucking bar before riveting process is completed, resulting in denting of the aircraft skin or damage to rivet (smiley); 3) countersinking the aircraft skin too deeply, causing the rivet gun header to contact the skin instead of the rivet and introducing fatigue cracks in the skin; 4) communication errors between rivet team members who cannot see one another and work in a noisy environment resulting in denting of the aircraft skin.

According to riveting instructors, these are the most commonly made errors by students in the Department of Aviation Technology at Purdue University. When a physics-based model of the nonlinear dynamic operator–tool–part interactions are developed, a metric for identifying one or more of these four errors in actual riveting can be defined, and a measurement system can be designed to assess real-time process quality.

A. Physics-Based Model

Figure 2 shows the proposed simplified model of the operator, rivet, gun, and part consisting of the following set of parameters: 1) gun mass M_g with displacement x_g; 2) piston rod mass M_d with displacement x_d; 3) rivet/part mass M_r with displacement x_r; 4) gun operator stiffness K_h, isolator stiffness K_i, stiffness at rivet head K_r, and stiffness at bucking bar K_b; 5) pneumatic force $f(t)$; and 6) two gaps at the front and back of the fuselage part to account for impacts during the riveting process when the preload varies with gun/bucking bar angularity and operator error.

This simplified model does not account for out-of-plane displacements of the gun or fuselage section, nor does the model incorporate

complicated damping mechanisms that exist due to the momentum transfer that occurs at the front and back interface of the rivet. Although the added complexity of these factors would improve model performance, the objective of this work was not to develop a fully descriptive quantitative model of the riveting process, but rather to study trends in the response spectrum of the gun M_g when the common riveting errors just mentioned occur during processing. These trends can then be utilized to extract features for assessing rivet process quality.

The equations of motion of this three-degree-of-freedom model are given here,

$$M_g\ddot{x}_g + (K_h + K_i)x_g - K_i x_d = 0 \tag{1a}$$

$$M_d\ddot{x}_d + K_i x_d - K_i x_g - g_2(x_d - x_r) = f(t) \tag{1b}$$

$$M_r\ddot{x}_r - g_1(x_r) + g_2(x_d - x_r) = 0 \tag{1c}$$

where the two nonlinear restoring forces, $g1$ and $g2$, are functions of the two gaps at the front and back of the rivet. These equations are straightforward to derive but difficult to analyze analytically. Therefore, a Simulink® model was generated as shown in Fig. 3 to analyze the response spectra.

All of the blocks in Fig. 3 are extracted directly from Eqs. (1a–1c), except for two bias displacement blocks that are used to enforce preloads provided by operators of certain magnitudes on the front and back of the rivet. These preloads can be varied to study the effects of harder or softer riveting operations. The exact values of these preloads were not relevant to this study, but rather changes in these preload forces were of importance because they can be used to model faults in the riveting procedure. Harder riveting results in fewer impacts because the preload between the tool, lap joint, and bucking bar is maintained. Softer riveting results in greater numbers of impacts because the gaps are permitted to open when the preload drops.

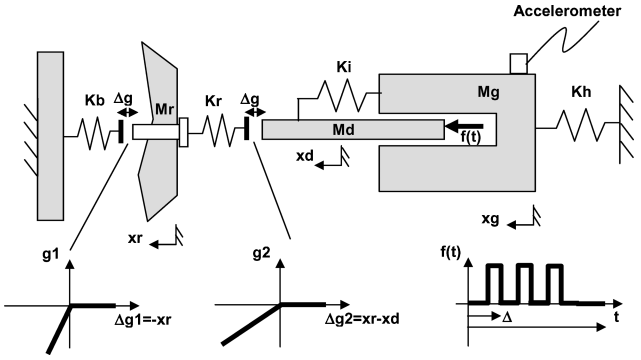

Fig. 2 Schematic of simplified rivet gun and tool interface model including gun, piston rod, rivet/part mass, and various boundary conditions along with two gaps at front and back of fuselage part.

The nominal parameter values selected in this simulation model are listed in Table 1. Note that two unique mass and stiffness parameters associated with the gun mass M_g and the operator stiffness K_h are selected, and then these parameters are used to compute the other model parameters. The model parameters were not selected to match exactly the riveting gun and process being studied; however, the parameter orders of magnitude are representative of experiments described later.

The parameters listed in Table 1 correspond to a riveting process of acceptable quality. The model will be used next to examine changes in the gun's dynamic response x_g to different types of riveting errors. A fixed-step Dormand–Prince integration technique was used to simulate the response.

B. Simulation Results

Figure 4a shows the time history and Fig. 4b the frequency domain spectrum of the forcing function due to the pneumatic piston within the rivet gun. A Hanning window was utilized to process time histories in all of the subsequent analysis to reduce frequency domain leakage in the frequency spectra shown. For a 40-Hz excitation, note that the frequency spectrum (Fig. 4b) has components at 40, 120, 200, and all odd multiples of 40 Hz. If the rivet gun model were linear, then it would respond at only these frequencies of excitation in the steady state; however, the simulation model in Fig. 3 is nonlinear, leading to additional response frequencies. Also note that because damping was not included in the simulation model, linear and nonlinear transients are present in the time and frequency domain data. The lack of damping is not the only reason that transients are present in the data; however, when the gun is damped, transients that occur during impacts vanish more quickly. The objective of these simulations is to determine the feasibility of characterizing rivet process quality, and so the presence of these transients is desirable; transient responses contain higher

Table 1 Parameters for nonlinear simulation of riveting process dynamics

Parameter	Value
M_g	8.8 kg
M_d	$M_g/5$
M_r	$M_g/10$
K_h	4.4e6 N/m
K_i	$K_h/4$
K_r	$K_h/2$
K_b	K_h
x_{r_bias} (to enforce preload)	1$e-$3 m
x_{d_bias} (to enforce preload)	3$e-$3 m
Time step Δt	30 ms
Simulation time T	3 s
Frequency resolution Δf	0.33 Hz
Forcing function amplitude A_f	2220 N (500 lb force)
Fundamental frequency of square function *ff*	40 Hz

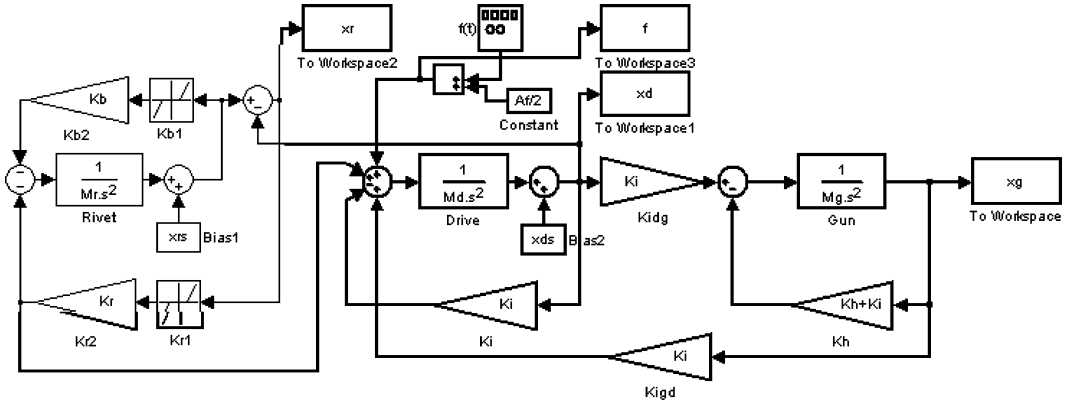

Fig. 3 Block diagram simulation model used to calculate three response degrees of freedom.

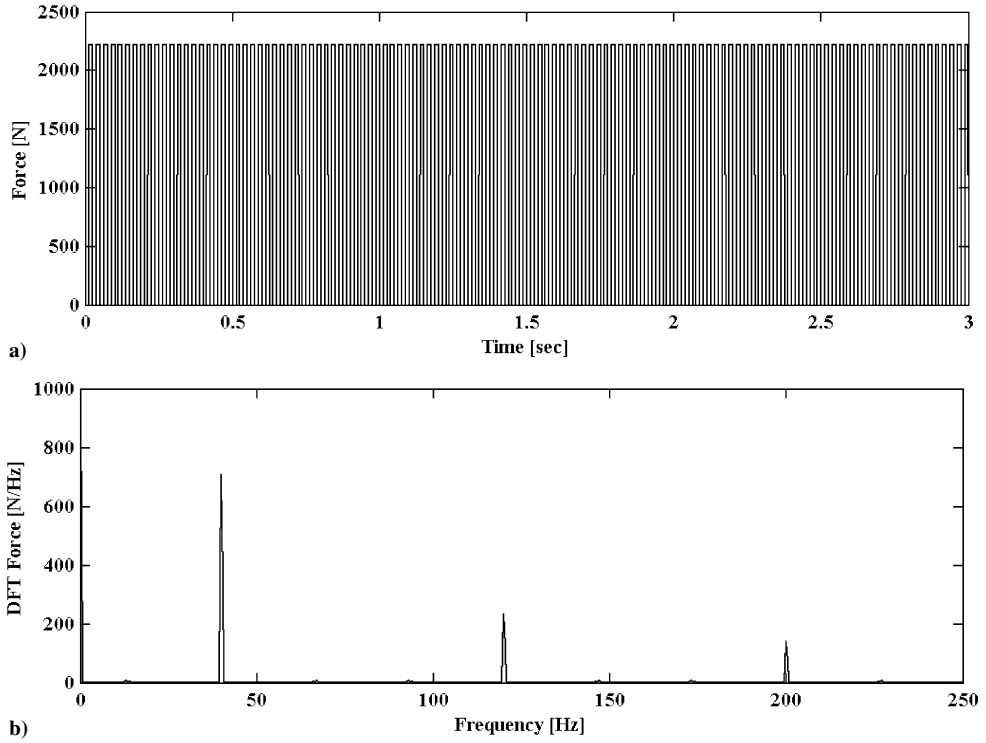

Fig. 4 Pneumatic excitation force $f(t)$ as a) function of time and b) frequency showing odd harmonics of 40-Hz fundamental frequency of excitation.

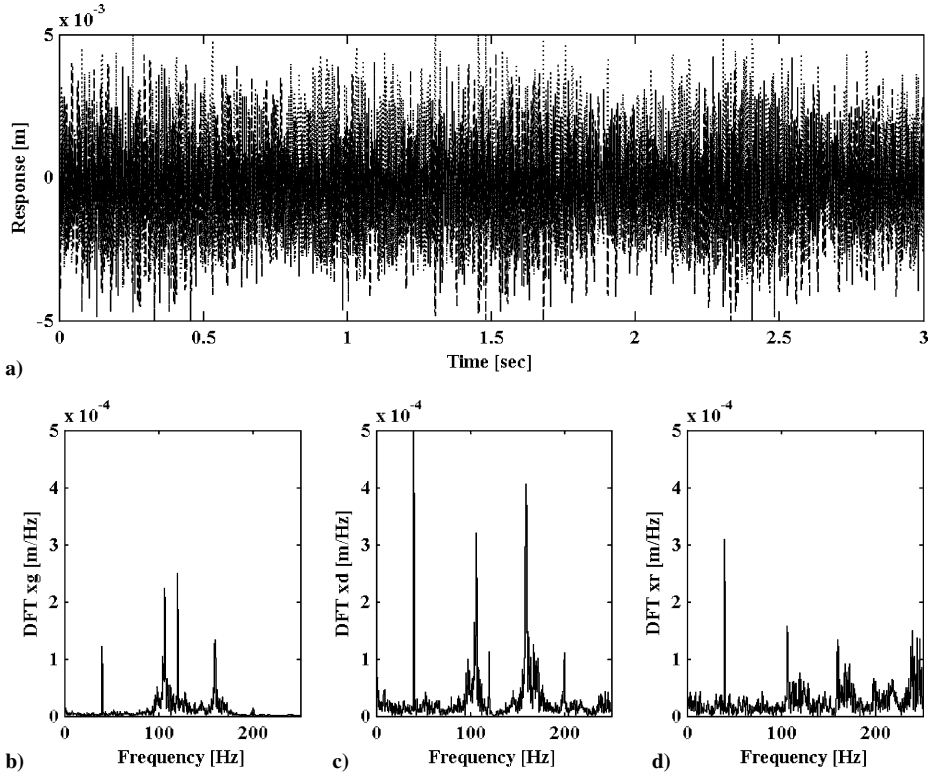

Fig. 5 Simulation results: a) x_g, x_d, and x_r responses as a function of time, b) frequency spectra showing response components at excitation frequencies, c) natural frequencies of rivet operator–gun–tool system, and d) nonlinear combinations of these frequencies.

bandwidths than steady-state responses and higher-bandwidth responses help in diagnosing processing quality.

Figure 5a shows the results of the simulation model in the time domain and Figs. 5b–5d in the frequency domain for the nominal parameters listed in Table 1. Note that riveting ram motion x_d has the largest magnitude response at 40 Hz, whereas the gun has the least response at that frequency due to the isolation spring in the rivet gun model. The motion at 100 Hz is a nonlinear resonant frequency of the system. The frequency is referred to as a nonlinear resonance because the frequency is largely a function of the gaps, which sometimes open and close, in front of and behind the rivet.

Next consider several simulations in which the parameters in Table 1 are modified to mimic errors in the riveting process. For example, if K_h is reduced by a factor of 0.5, the frequency domain simulation results in Fig. 6 are obtained for the three displacement coordinates. A reduction in K_h simulates a loss of preload as supplied by

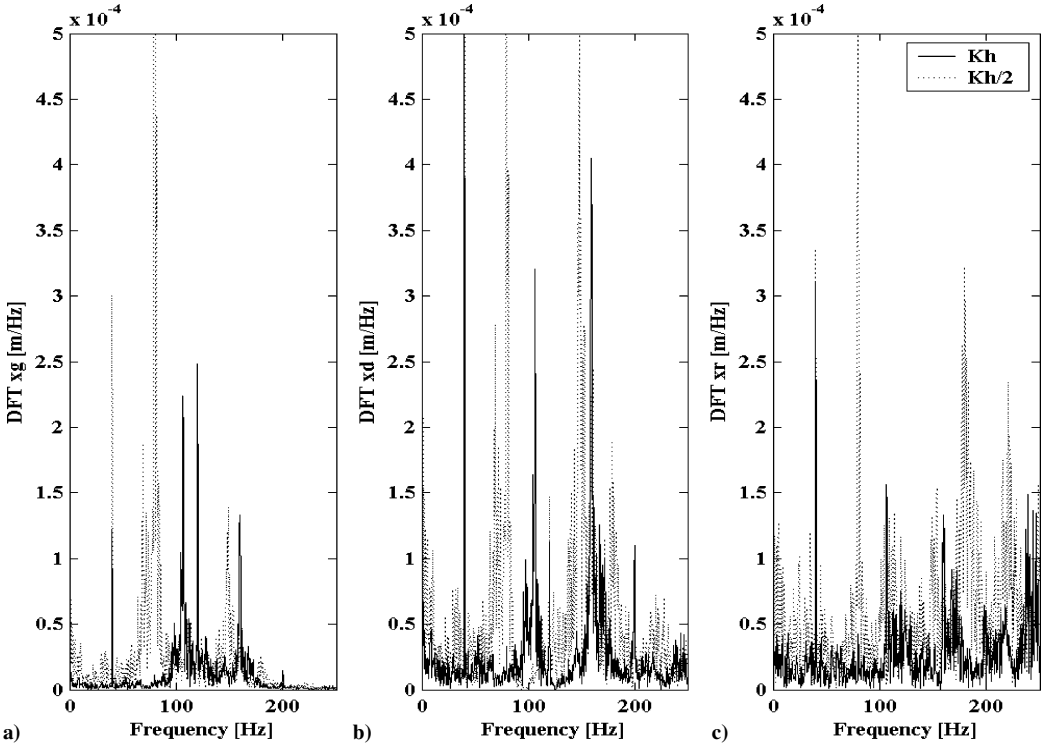

Fig. 6 Responses a) x_g, b) x_d, and c) x_r for ——, K_h and · · · ·, $K_h/2$ (Table 1) showing reduction in 100- and 160-Hz system nonlinear resonant frequencies due to loss in preload at rivet head.

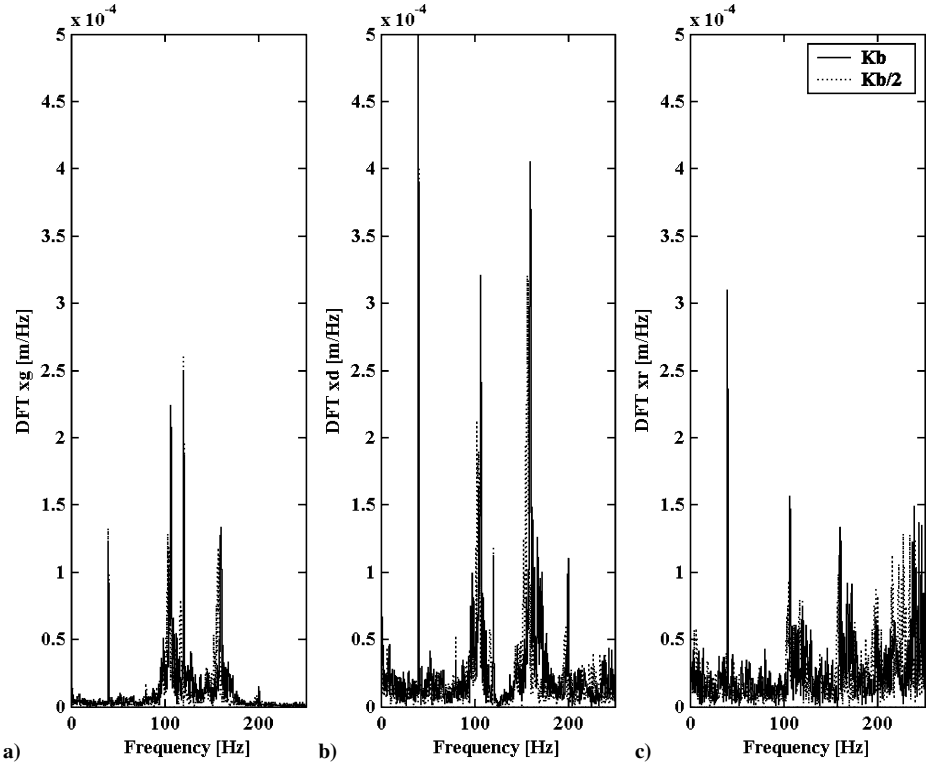

Fig. 7 Responses a) x_g, b) x_d, and c) x_r ——, K_b and · · · ·, $K_b/2$, showing relatively small reduction in 100- and 160-Hz system natural frequencies due to bucking bar slipping.

the operator. This loss of preload results in a reduction in the 100-Hz resonant frequency of the system to approximately 75 Hz and the 160 Hz resonance to 150 Hz due to the change in effective stiffness when the stiffness provided by the operator drops and the equilibrium point moves along the $g2()$ function. Recall the form of $g2$ in Fig. 2. When the equilibrium point shifts to the right on this function, the effective stiffness drops due to the intermittent loss of contact with the tool. When the motion of the gun x_g is monitored, (Fig. 6a), it is expected that these shifts in nonlinear resonant frequencies will be evident in acceleration data acquired on the rivet gun.

Next consider the case when the bucking bar is angled or slips during the riveting process. A reduction in the stiffness provided by the bucking bar is used to simulate this case. When the stiffness provided by the bucking bar drops, there are only small changes in the system resonant frequencies, as seen in Fig. 7, leading to inconclusive evidence that the bucking bar was repositioned. It is

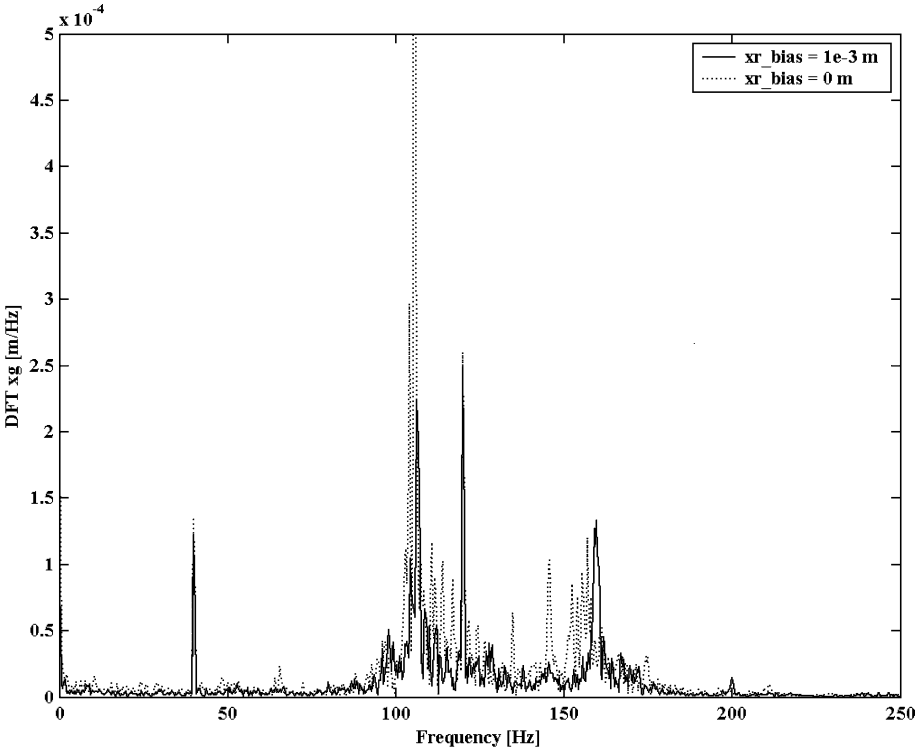

Fig. 8 Frequency spectrum x_g for two different values of x_r_bias (x_r_bias from Table 1 and x_r_bias = 0 mm), showing reductions in 100- and 160-Hz system natural frequencies.

believed that the drop in bucking bar preload is not evident in the simulation response data because of the distance of this boundary condition from the rivet forcing function. Attenuation due to the impact events results in a less clear indication of the loss in preload at the bar.

If the gun is repositioned relative to the rivet head to reduce the preload force, then this type of error in the riveting process can be modeled by changing the bias displacement, x_{r_bias}. For example, when x_{r_bias} is reduced, the result in Fig. 8 is obtained for the frequency spectrum of the gun displacement x_g. Note that again the reduction in preload causes a reduction in the nonlinear resonant frequencies near 100 and 150 Hz. These kinds of reductions in nonlinear resonant frequencies will be utilized in the following experiments to assess rivet process quality.

Numerous other cases can also be simulated, but all cases led to the same conclusion: change in preload provided by the gun, bucking bar operator stiffness, or bias displacement lead to reductions in stiffness and the nonlinear resonant frequencies of the system. In the next section, experiments are performed and frequency domain features are extracted from the measured data to assess rivet process quality.

C. Experimental Data Analysis Approach

Experiments were performed on the rivet gun shown in Fig. 1a to measure shock vibration data in three directions to distinguish good-quality riveting from poor-quality riveting (Fig. 9a). Different operators who use the rivet gun and bucking bar have a different feel for the riveting process; therefore, it is essential that good- and bad-quality rivets from the perspective of different riveters be used to produce statistically meaningful results. To capture this variability, data were acquired as different professionally trained riveters from the Department of Aviation Technology at Purdue University performed good- and bad-quality riveting. The data were then processed simultaneously to draw from a population of operators with different sensitivities. Although two to three riveting teams, each consisting of two operators, one on the gun and one on the bucking bar, were included in this study, more operators in the dozens would be needed to identify precise statistical properties of the distribution that describes operator-to-operator variability.

Piezoelectric shock accelerometers are shown installed in Fig. 9a near the rear of the gun to avoid interference with the operator on the handle or the tool–part interface at the rivet. Low-sensitivity shock accelerometers were used in experiments to avoid clipping of the response signal and damage to the piezoelectric elements. Note that because of the low-sensitivity nature of these sensors, certain features evident in the analytical simulation results would not be observable in the experiments. Three dynamic time domain acceleration measurements in the X, Y, and Z directions for each riveting operation were then transformed into the frequency domain using the discrete Fourier transform (DFT). The DFT $Q_m(n\Delta f)$ can be represented as follows for a sampled and windowed time history $q_m(k\Delta t)$, BS time samples in length:

$$Q_m\left[\frac{n}{BS\Delta t}\right] = \sum_{k=0}^{BS-1} q_m(k\Delta t)e^{-j2\pi nk/BS}$$

$$m = 1, 2, 3, \qquad n = 0, 1, 2, \ldots, BS-1 \quad (2)$$

where m denotes the DFT for the X, Y, or Z direction data and n denotes the frequency value at frequency resolution $\Delta f = 1/BS\Delta t$. DFTs were computed using the fast Fourier transform algorithm in MATLAB® with a Hanning window on $q_m(k\Delta t)$.

Once the complex-valued DFT spectra in the three coordinate directions were computed, features F_p were extracted for one or more frequency bands ($n_{p,\min}$, $n_{p,\max}$),

$$F_p = \sum_{n_{p,\min}}^{n_{p,\max}} \sum_{m=1}^{3} \left\| Q_m\left(\frac{n}{BS\Delta t}\right)\right\| \quad (3)$$

Feature objects (curves, planes) were then generated with parameter sets in Cartesian coordinates space (F_1, F_2, ...) and geometrical objects (lines, circles, ellipses) were curve fit to the feature space to separate acceptable and unacceptable rivet processes with some confidence interval. For example, a displaced and rotated elliptical cluster of features in two-dimensional parameter space is described with the expression,

$$\left(\hat{F}_1^2/a^2\right) + \left(\hat{F}_2^2/b^2\right) = 1 \quad (4a)$$

where

$$\begin{Bmatrix} F_1 - \alpha \\ F_2 - \beta \end{Bmatrix} = \begin{bmatrix} \cos\theta & -\sin\theta \\ \sin\theta & \cos\theta \end{bmatrix} \begin{Bmatrix} \hat{F}_1 \\ \hat{F}_2 \end{Bmatrix} \tag{4b}$$

where a and b denote the major and minor axes of a translated and rotated ellipse that contains features for acceptable rivet processes, α and β denote the displaced parameter space coordinate system for the ellipse, and θ denotes the angle through which the ellipse is rotated. The carats denote the transformed set of geometric coordinates.

To account for variability due to gun dynamics, the frequency response function (FRF) between the force at the rivet plate and the acceleration responses on the barrel (Fig. 1b) were measured for each gun. Figure 9b shows an axial (Z direction) FRF for the rivet gun used in these tests. FRFs for all guns showed negligible flexible body dynamics in the frequency range of interest, that is, the FRFs all asymptotically approached a constant at DC, the value of which is the reciprocal of the effective mass of the gun; therefore, it was only necessary to multiply raw acceleration data by the effective gun mass M_{gun} to remove the variability in the features from Eq. (3) due to differences in gun dynamics. This multiplication changes the DFT amplitudes throughout the 0–200 Hz range. In other words, large feature values for heavier guns are given more weight than corresponding values for lighter guns. No data for additional guns were acquired to verify that the gun-to-gun variability in quality assurance features has actually been removed. Note that the gun used in these tests had an isolation spring in the butt of the gun.

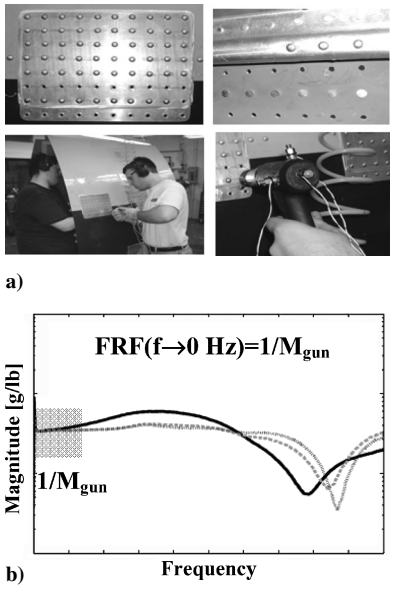

Fig. 9 Photographs of a) structural component with rivets (front/back), two-person riveting team, and instrumented gun, and b) modal impact FRF magnitude for rivet gun in axial direction showing flat response in low-frequency range.

IV. Experimental Procedure

Three PCB U350B02 shock integrated charge piezoelectric (ICP) accelerometers (0.1 mV/g) were installed on the barrel of the gun (Fig. 9a). Size 6 rivets with universal head (BACR15CE5D6 reduced countersink and MS20470AD6-6 protruding) were used in the experiments along with a recoilless US4R rivet gun from U.S. Industrial Tool and Supply Company. The fuselage section used in this study is based on the Boeing 737 with 0.050-in. 2024T3 aluminum alloy and stringers/frames of 7075T6 aluminum alloy. An IOTech Waveport™ data acquisition system was used to acquire 1e4 samples of time history data at a 10-kHz sample rate with a 5000-Hz analog low-pass filter and 2 mA of ICP current. The riveters performed five good operations intermixed with poor-quality operations including 1) gun at 10 deg with respect to the normal; 2) bucking bar at 10 deg with respect to the normal; 3) circular indentations, so-called smileys, after completing the rivet; and 4) bucking bar slippage midway through the rivet.

V. Results

The results of the experiments are shown in Figs. 10a–10e. Each plot in Fig. 10 shows the magnitude of the DFT coefficients [Eq. (2)] for the corresponding set of rivets with the same qualitative assessment. There is significant spectral content in the two bands of 65–75 and 88–112 Hz for the good-quality rivets that is largely absent in

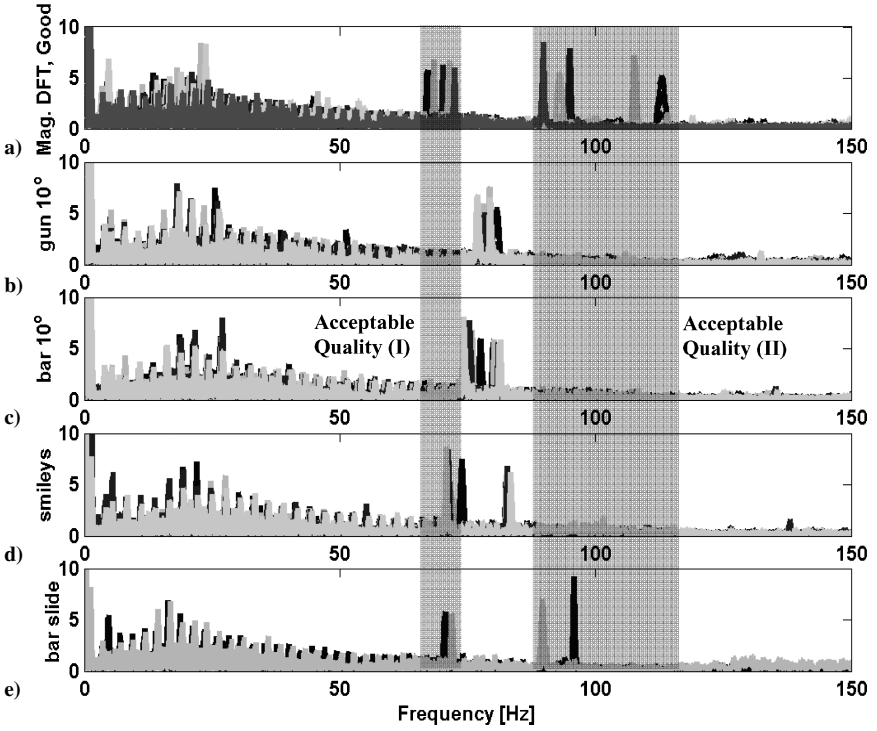

Fig. 10 Magnitude of DFT coefficients measured for size 6 rivet universal head for a) five good-quality rivets, b) four rivets with gun skewed by 10 deg, c) four rivets with bucking bar skewed by 10 deg, d) four rivets producing smiley pattern, and e) two rivets with bucking bar slip; shaded regions, 1 and, 2 of spectral features indicating acceptable rivet process quality are shown.

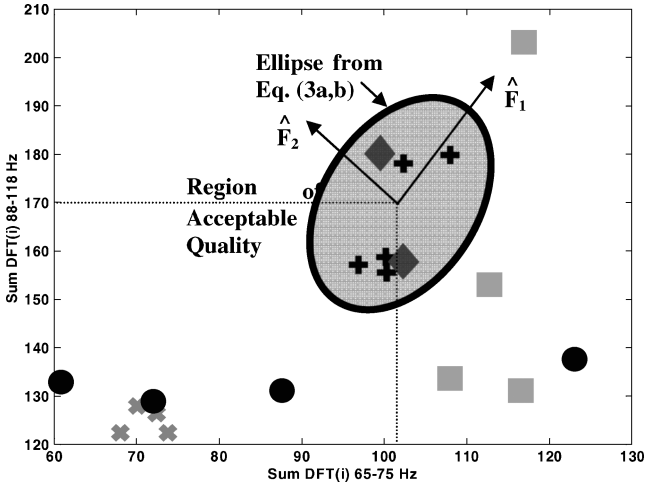

Fig. 11 Two-dimensional feature space for DFT summation for 88–112 Hz frequency band vs DFT summation for 65–75 Hz band with +, good-quality rivets; ×, gun skewed; ○, bucking bar skewed; ■, smiley pattern; and ◇, bucking bar slip showing elliptical clustering with all missed diagnoses of poor-rivet processes for bucking bar slippage.

the spectra of the poor-quality rivets; these frequency bands are shaded to highlight the visual comparisons between Fig. 10a and Figs. 10b–10e. The spectra for good-quality rivets in Fig. 10a resemble the K_h spectra in Fig. 6 for good-quality rivets in the simulation model. Specifically, there are two ranges of spectral peaks surrounding 100 Hz in the simulation data, and these peaks are also present in the experimental data. The peaks near 75 Hz in the experimental data are closer to 50 Hz in the simulation model data and likely account for a harmonic of the pneumatic driving frequency. Differences in the nonlinear resonant frequencies can be attributed to errors in the part stiffness, pneumatic driving forcing function (where an idealized square wave pulse was used in the simulation model), and other parameters in the simulation model.

Note that in the first four poor-quality riveting operations, the DFT spectra lack the appropriate frequency content in the first, second, or both frequency bands. This trend was observed for the individual X, Y, and Z spectra even though the X spectra has the smallest DFT magnitudes due to its vertical orientation on the barrel. In the case of bucking bar slippage, the results are inconclusive, perhaps because slippage occurred toward the end of the process. Recall that the nonlinear model simulation (Fig. 7) was also inconclusive when the stiffness at the bucking bar dropped. It is believed that this change due to bucking bar slippage affects the DFT coefficients less than the other conditions because of the filtering properties of the fuselage section on the riveting dynamics.

By comparison of the results in Fig. 10 with those in Figs. 6 and 8, the differences in the spectra for riveting processes of varying quality can be attributed at least partially to differences in applied preload, which is difficult to properly maintain when the gun and/or bucking bar are/is skewed, and partly to an excessive preload in the case of the circular indentations that are left behind following the rivet processes. A preload that is too small seems to cause a lack of higher-order harmonics in the spectra (Figs. 10b and 10c) because the interface force is intermittent. In contrast, a preload that is too large causes a decrease in the separation between harmonics, resulting in the spectral peaks falling between the bands of acceptable quality. These conclusions are both supported qualitatively by the simulations conducted using the nonlinear model in Fig. 2.

To quantify the differences observed in Fig. 8, the rivet quality features in each of the frequency bands in Eq. (3) were computed for each rivet process. The two-dimensional parameter space, Cartesian coordinates (F_1, F_2) from Eq. (3) for $p = 1$ and 2, summarizing these results is shown in Fig. 11. The plus symbols denote the good-quality rivets, and the poor-quality rivets are denoted with × for gun skewed cases, ○ for bar skewed cases, ■ for smiley pattern cases, and ◇ for bar slippage cases. Note that all poor-quality rivet operations other than the bar slippage case are correctly classified using an elliptical object in the two-dimensional plane. An ellipse (circle) that bounds the good-quality rivets was also generated using Eqs. (4a) and (4b) with $\alpha = 102$, $\beta = 170$, $\theta = 50$ deg, $a = 10$, and $b = 10$ (Fig. 11, solid line).

VI. Conclusions

It was demonstrated using rivet quality assurance indicators based on vibration-based spectral transmission through the tool–part interface and human operator specifications that frequency domain data interrogation techniques can be utilized to identify riveting processes with skewed delivery (gun or bar), circular indentations, and bucking bar slip and, thus, identify susceptibility to future material damage near rivet holes in fuselage structures. A physics-based nonlinear model of the operator–gun–tool system was developed to support the experimental conclusions. To verify that this approach could be used for the purpose of guiding NDE inspections as intended, fatigue tests will need to be conducted in future work to identify future damage sites by applying static and dynamic forces to a fuselage section with varying degrees of rivet quality. Future work will also more rigorously examine the variability from riveter to riveter, from rivet to rivet, and from gun to gun.

References

[1]Petrak, G. J., and Stewart, R. P., "Retardation of Cracks Emanating From Fastener Holes," *Engineering Fracture Mechanics* Vol. 6, No. 2, 1976, pp. 275–282.

[2]Cathey, W. H., and Grandt, A. F., "Fracture Mechanics Considerations of Residual Stresses Introduced by Cold Working Fasteners Holes," *Journal of Engineering Materials and Technology*, Vol. 102, Jan. 1980, pp. 85–91.

[3]Reid, L., "Split Sleeve Cold Expansion as a Rework Process for Previously Cold Expanded Holes," *Proceedings of the 17th Symposium of the International Committee on Aeronautical Fatigue*, Vol. 2, 1993, pp. 1121–1139.

[4]Ryan, L., and Monaghan, J., "Failure Mechanism of Riveted Joint in Fiber Metal Laminates," *Journal of Materials Processing Technology*, Vol. 103, No. 1, 2000, pp. 36–43.